Self-Propagative Multi-Task Learning for Predicting Cardiometabolic Risk Factors

Seonghyeon Ko[1], Huigyu Yang[2], Junghyun Bum[3], Duc-Tai Le[4], and Hyunseung Choo[4]*

[1] Dept. of AI Systems Engineering, Sungkyunkwan University, South Korea
[2] Convergence Research Institute, Sungkyunkwan University
[3] Sungkyun AI Research Institute, Sungkyunkwan University
[4] Dept. of Electrical and Computer Engineering, Sungkyunkwan University
{shko0215, huigyu, bumjh, ldtai, choo}@skku.edu
*Corresponding author: Hyunseung Choo

Abstract. CardioMetabolic Risk (CMR) assessment requires numerous risk factors derived from anthropometric measurements, sphygmomanometry, and blood tests. Deep Learning enables CMR factors to be acquirable from a medical image (e.g., fundus), however, model-per-factor approach is insufficient solution in cost-efficiency. It is also challenge to predict multiple factors simultaneously from a single image, since the CMR factors are inter-correlated among themselves but also correlated with fundus features in various depths. To address this challenge, we propose Self-Propagative multi-task Learning (SePL) which utilizes comparatively simple 6 CMR factor predictions as prior knowledge to guide predicting more complex CMR factors. The proposed SePL propagates its initial predictions to a latent space, enriching unimodal features into multimodal representation. A discriminative mixture of experts leverages the relevant prior for 9 CMR factor predictions. The training and testing of SePL use 5,232 sets of fundus images and corresponding CMR factors. Experimental results demonstrate that the proposed SePL outperforms the existing methods up to 10.46% of AUC and 8.07% of MAE across all 15 CMR factor predictions. The code is available at https://github.com/shko0215/SePL.

Keywords: Self-Propagation · Discriminative Mixture of Experts · Multi-task Learning · Multimodal Learning

1 Introduction

CardioMetabolic Risk (CMR) assessment requires anthropometric screening, sphygmomanometry, and blood test to measure CMR factors [3, 7, 17]. The examinations are costly and invasive, and the result is variable depending on the examinee condition [14, 15]. Recent advances in Deep Learning (DL) techniques shed light on non-invasive CMR factor acquisition [5, 6, 13], however, deriving diverse CMR factors from single image is challenging due to their heterogeneous nature and disparate levels of inter-factor dependencies. The diversity of CMR

prediction task and correlation leads existing studies to design task-wise DL networks. This Single-Task Learning (STL) approach necessitates separate networks for each CMR factor, resulting in increased computational complexity and redundancy for comprehensive CMR assessment. To this end, a novel method for CMR factor prediction is necessary to leverage inherent correlations among CMR factors while reducing computational cost.

Previous studies on DL-based CMR factor prediction have predominantly relied on STL, treating each factor as an independent modeling task. The first DL approach utilizes Inception-v3 to predict gender, age, Systolic/Diastolic Blood Pressure (SBP/DBP), Body Mass Index (BMI), HbA1c, and smoking status [13]. The six individual models undergo 10 times of sampling and outputs average for each factor, leading to excessive computational overhead. Comprehensive CMR factor prediction adopts Mobilenet-v2 to mitigate high computational costs for predicting relative fat mass, glucose, insulin, sex hormone binding globulin, estradiol, testosterone, total/HDL/LDL-cholesterol, and triglyceride in addition to previous study [5]. The model outputs are averaged over 4 different fundus images per person, without reducing the number of models per factors. Systemic health features are predicted with Densenet-201 by switching 4 regression tasks to binary classification tasks [6]. The comprehensive CMR assessment is limited to binary outputs of various factors. Previous studies struggle to integrate dozens of classification and regression tasks, extract task-wise features from single data source, and utilize the inter-factor correlations.

To address these challenges, we propose Self-Propagative multi-task Learning (SePL) for enriching single-source features by propagating prior knowledge to simultaneously predict 15 CMR factors. A shared feature extractor learns robust feature representation from fundus images, while significantly decreasing network size. Anthropometric heads initially predict 6 CMR factors. Anthropometric measures are relatively simple to predict, as these are readily available and have correlation [4, 8, 13]. Self-propagation utilizes these initial predictions to serve as prior knowledge for subsequent 9 CMR factor estimations, leveraging the intrinsic relation between the priors and the other CMR factors [1, 2, 10]. Discriminative Mixture of Expert (DMoE) fusion selectively integrates image features and anthropometric prior to generate enriched feature representations. Task-specific gating networks employ a soft-gating strategy to aggregate diverse perspectives of enriched feature representations. Each selective expert network learns a unique combination of multimodal feature representations. The remaining task heads receive a weighted sum of expert outputs to predict 9 additional CMR factors. The main contributions are as follows:

1. To the best of our knowledge, this study is the first to integrate multi-task learning, multimodal learning, and mixture of experts for comprehensive CMR factor prediction.
2. The proposed self-propagation first predicts a subset of CMR factors and utilizes these predictions to enhance signle-source features. The complex CMR factors benefit from multimodal feature representations without requiring additional input.

3. The proposed DMoE fusion enables the network to selectively combines image feature with propagated prior knowledge, providing discriminative feature representation for complex CMR factors.
4. Our comprehensive experimental evaluation demonstrates that the proposed SePL surpasses state-of-the-art methods across 15 CMR factor predictions with reduced computational costs. This enables broader prediction coverage for comprehensive DL-powered CMR assessment in a lightweight manner.

2 Methods

2.1 Dataset and Data Preprocessing

A total 5,232 sets of de-identified fundus image pairs and corresponding CMR factors are collected from people who visited the Health Promotion Center at Ajou University Hospital between January 2020 and June 2020. The fundus images have a resolution of $[2592 \times 1728]$ in DICOM file format. CMR factors are obtained from blood tests, and their basic statistics are summarized in Table 1. This study was approved by the Institutional Review Board (IRB) at Ajou University Medical Center (AJOUIRB-DB-2024-330).

Table 1: Descriptive statistics of CMR factors in Ajou dataset

	Gender	**Age** (year)	**Weight** (kg)	**Height** (cm)	**BMI** (kg/m^2)	**Waist** (cm)	**SBP** (mmHg)	**DBP** (mmHg)
Mean	Male:	49.77	67.94	167.03	24.22	85.90	115.91	74.18
Std	3,218	10.61	12.58	8.59	3.24	7.88	13.99	10.44
Min	Female:	19	34.20	141.30	14.60	60.20	74.00	43.00
Max	2,014	89	144.80	192.80	41.80	130.00	190.00	114.00

	T-chol (mg/dL)	**TG** (mg/dL)	**Glucose** (mg/dL)	**BUN** (mg/dL)	**Creatinine** (mg/dL)	**Uric Acid** (mg/dL)	**HbA1c** (%)
Mean	193.83	128.12	99.15	11.73	0.87	5.30	5.69
Std	37.25	78.64	18.96	3.54	0.23	1.37	0.68
Min	81.00	22.00	53.00	3.90	0.39	0.60	4.50
Max	458.00	988.00	344.00	77.60	10.83	11.00	12.50

CMR factors consist of gender and 14 continuous factors. Gender is encoded as a binary variable, where 0 and 1 indicate female and male, respectively. Continuous factors have different scales and contain outliers, as shown in Table 1. The scale disparity causes imbalanced model convergence across CMR factors, as large-scale factors dominate the total loss. We standardize continuous CMR factors with the interquartile range, which is less sensitive to extreme values [12,16]:

$$y_{\text{scaled}} = \frac{y - Q_2(y)}{Q_3(y) - Q_1(y)}, \tag{1}$$

where Q_1, Q_2, and Q_3 are the first, second (median), and third quartiles of each CMR factor y in the training set. This transformation reduces disparities across CMR factors while mitigating the impact of outliers, as illustrated in Fig. 1.

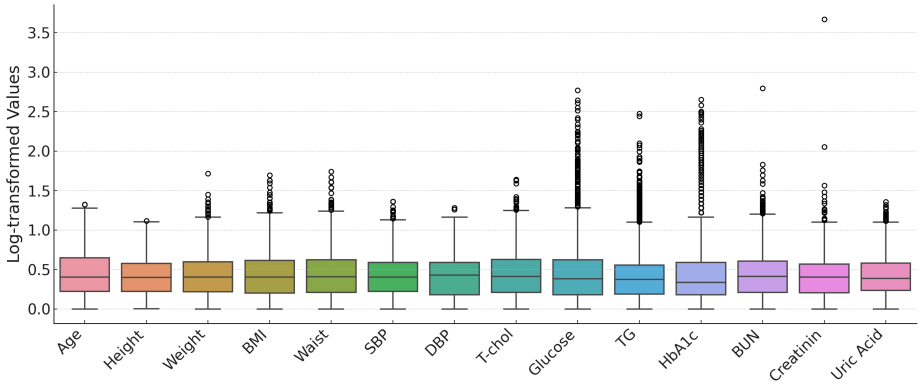

Fig. 1: Distribution of scaled results for 14 continuous CMR factors. Log transformation is applied to enhance clarity and readability for visualization.

Fundus image quality varies due to participant-related factors (e.g., eyelashes, blinking) and lighting conditions. Low-contrast images obscure important fundus structures such as blood vessels, optic disc, macula, fovea, and retina. It is a challenge to predict various CMR factors with limited features of single fundus image. We adopt Contrast Limited Adaptive Histogram Equalization (CLAHE) to enhance local contrast and mitigate illumination inconsistencies [18, 19]. The resultant images undergo resizing $[256 \times 256]$ and center-cropping $[224 \times 224]$ to decrease computational cost and remove unnecessary background pixels.

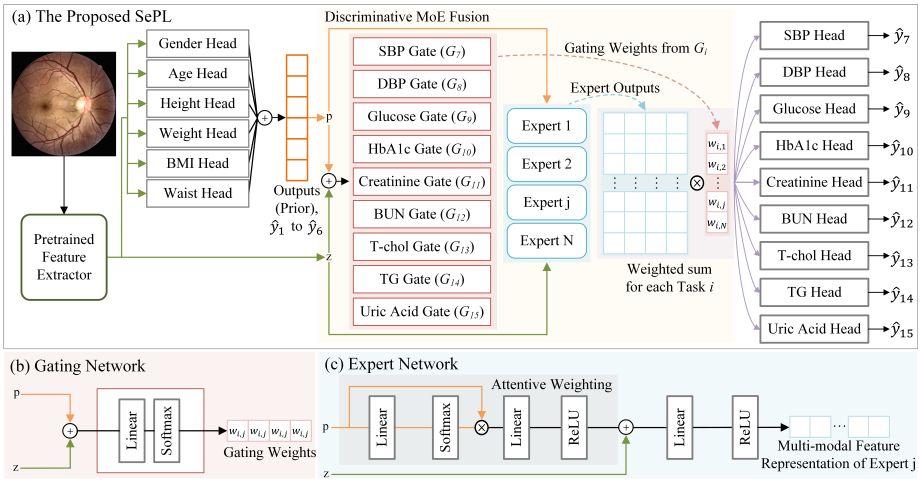

Fig. 2: The overall architecture (a) of the proposed SePL. The gating network and expert network are illustrated in (b) and (c), resepectively.

2.2 Preliminary: Multi-task Definition

This study aims to design a lightweight DL model capable of simultaneously predicting 15 distinct CMR factors from a single fundus image, as illustrated in Fig. 2(a). Let the set of tasks be denoted as $\{T_i\}_{i=1}^{15}$. The task T_1 is formulated as a gender classification problem with the corresponding label $y_1 \in \{0, 1\}$. The tasks $\{T_i\}_{i=2}^{15}$ are defined as regression problems, each associated with a continuous label $\{y_i\}_{i=2}^{15} \in R$. The tasks are categorized into two groups: the anthropometric factor predictions $\{T_i\}_{i=1}^{6}$ (gender, age, height, weight, BMI, waist circumference), and the complex CMR factor predictions $\{T_i\}_{i=7}^{15}$.

2.3 Feature Extraction and Anthropometric Prior Prediction

The feature extractor $F(\cdot)$ takes a fundus image $x \in R^{H \times W \times C}$ to produce a high-dimensional feature representation $z = F(x)$, where $z \in R^d$. Each anthropometric head predicts a single anthropometric factor from z:

$$\hat{y}_i = W_i z + b_i, \quad i \in \{1, \ldots, 6\}, \tag{2}$$

where W_i and b_i are learnable parameters for each anthropometric head to predict $\{T_i\}_{i=1}^{6}$. The prediction outputs $\{\hat{y}_i\}_{i=1}^{6}$ are concatenated into single-dimensional vector, forming the anthropometric prior knowledge p. The image feature z and prior p are propagated into Discriminative Mixture of Experts (DMoE) fusion module to extract enriched feature representations for predicting more complex factors $\{T_i\}_{i=7}^{15}$.

2.4 Discriminative Mixture of Experts

Gating Network The gating network is designed to evaluate the multimodal features and dynamically assigns soft weights to expert networks, as shown in Fig. 2(b). This soft mixture approach ensures that all experts contribute to the complex CMR factor prediction tasks $\{T_i\}_{i=7}^{15}$ with varying importance. Each task-specific gating network G_i maps both the image feature z and anthropometric prior p into multimodal feature space, yielding a gating weight w_{ij}:

$$w_{ij} = \mathrm{Softmax}\big(G_i(z, p)\big), \tag{3}$$

where G_i consists of learnable parameters W_i and b_i. The gating weight w_{ij} represents the contribution of expert E_j in predicting a specific CMR factor T_i. The gating network learns optimal contribution of each expert network to a given CMR factor, ensuring that relevant feature representations are prioritized.

Expert Network The expert network specializes in learning a subset of CMR factors with propagated multimodal features, as illustrated in Fig. 2(c). The calibration of anthropometric prior is necessary, as the contribution of each anthropometric attribute is dissimilar to predicting different CMR factors. The

attentive weighting mechanism is designed to dynamically determine which attributes are most relevant for each expert E_j:

$$p_j = \mathrm{ReLU}\Big(W_2\Big(\mathrm{Softmax}(W_1 p + b_1) \otimes p\Big) + b_2\Big), \tag{4}$$

where $\otimes$ denotes element-wise multiplication, and p_j is the calibrated prior for expert E_j. The individual expert E_j maps the image feature z and calibrated prior p_j, generating enriched feature representation m_j:

$$m_j = E_j(z, p_j), \tag{5}$$

where E_j comprises learnable parameters W_j and b_j, followed by ReLU activation function. Each expert E_j produces j different multimodal feature representations, which are later combined by weighted fusion.

Discriminative Fusion and Self-propagative Prediction The final feature representation h_i for each remaining task $\{T_i\}_{i=7}^{15}$ is obtained by a weighted sum of gating weights w_{ij} and multimodal representations m_j:

$$h_i = \sum_{j=1}^{K} w_{ij} m_j, \quad i \in \{7, \ldots, 15\}, \tag{6}$$

The gating weights are modified according to the specific anthropometric attributes which are most relevant to the target tasks $\{T_i\}_{i=7}^{15}$. This discriminative mixture of experts fusion ensures that the model benefits from multiple expert opinions while adapting dynamically to specific task requirements. The fused feature h_i undergoes task-specific heads to generate the predictions for $\{T_i\}_{i=7}^{15}$ via $\hat{y}_i = W_i h_i + b_i$, where W_i and b_i are learnable parameters.

2.5 Loss Function

The proposed SePL is trained in an end-to-end manner by aggregating the task-specific losses. The total loss L among the ground truth y_i and prediction $\hat{y}_i$ of T_i is computed as:

$$L = \sum_{i=1}^{15} L_i(y_i, \hat{y}_i), \quad L_i = \begin{cases} -\left[y_1 \log\left(\sigma(\hat{y}_1)\right) + (1 - y_1) \log\left(1 - \sigma(\hat{y}_1)\right)\right] \\ \frac{1}{N} \sum_{j=1}^{N} \left| y_i^{(j)} - \hat{y}_i^{(j)} \right|, \quad \text{for } i = 2, \ldots, 15, \end{cases} \tag{7}$$

where N is the number of samples, j indexes individual samples, and σ indicates the sigmoid function. BCE with Logits Loss aims to solve gender classification task, whereas MAE Loss targets to minimize discrepancy between y_i and $\hat{y}_i$. MAE is chosen over MSE to reduce sensitivity to outliers. Weighted loss strategy is not adopted, as we scaled the CMR factors in the preprocessing stage.

3 Results

3.1 Experimental Setting

Our experiments divide 5,232 set of fundus images and CMR factors into training, validation, and test subsets with a ratio of 7:1:2. The proposed SePL adopts ConvNeXt [11] as a feature extractor and 4 experts for DMoE fusion. Model training utilizes Adam optimizer [9] with a learning rate of 1×10^{-4} and batch size of 64 for 100 epochs. An early stopping algorithm prevents the model overfits to training set, by terminating the training process when the validation loss increases for five consecutive epochs. Our proposed method is implemented with PyTorch and CUDA libraries on a hardware environment comprising an Intel i9 CPU, 32GB RAM, and RTX 3090Ti GPU.

The proposed SePL is compared to the previous state-of-the-art methods [5, 6, 13]. The performance evaluation utilizes Accuracy (Acc) and Area Under the ROC Curve (AUC) for a gender classification task, and Mean Absolute Error (MAE) and Root Mean Squared Error (RMSE) for 14 regression tasks. We also calculate the FLoating point Operations Per Second (FLOPS) and the number of parameters to evaluate computational costs.

3.2 Experimental Results

The proposed SePL consistently outperforms STL baselines across all CMR factors, as represented in Table 2. Gender classification task benefits from combined supervision of Multi-Task Learning (MTL) framework. The SePL achieves an Acc of 87.30% and an AUC of 0.8635, representing 9.72% and 10.46% improvements compared to the second best method, respectively. The shared feature extractor learns more robust and enriched feature representation by aggregating gradient signals from 15 prediction tasks. Our proposed method consistently improves MAE 8.07% and RMSE 5.46% in average among the 14 regression tasks, compared to the second best method. Creatinine shows the highest improvement with MAE 18.18% and RMSE 12.50%, whereas waist circumference shows the lowest improvement with MAE 0.94% and RMSE 0.11%. It is worth noting that the proposed SePL improves 336.58% and 318.71% in the number of parameters and GFLOPs, respectively.

In-depth performance analysis indicates that the MTL and self-propagation with DMoE operate as intended. The anthropometric CMR factors indicate MAE 8.45% and RMSE 7.43% enhancements in average, surpassing the second best method. Direct supervision of the shared feature extractor facilitates more precise learning for these tasks. The other CMR factors also denote MAE 7.50% and RMSE 4.54% in average, outperforming the second best method. The performance gain is lower than anthropometric factors, since the other factors are predicted with self-propagated anthropometric priors which are model predictions. The predicted values inherently contain errors, introducing additional noise into the DMoE fusion. The relatively lower RMSE improvement demonstrates the affect of noise, as it is sensitive to larger deviations.

Table 2: Performance comparison of different methods on Ajou dataset. The **best** and second best results are highlighted.

	Metrics	Inception v3 [13]	Mobilenet v2 [5]	Densenet 201 [6]	Proposed SePL
Gender	Acc (AUC)	76.21% (0.74)	79.56% (0.77)	77.27% (0.75)	**87.30%(0.86)**
Age	MAE (RMSE)	13.99 (15.32)	3.67 (4.88)	3.60 (4.89)	**3.34** (**4.40**)
Height		43.39 (44.14)	6.26 (7.95)	6.40 (8.08)	**5.60** (**7.12**)
Weight		13.77 (17.42)	10.29 (12.83)	10.69 (13.48)	**8.99** (**11.80**)
Waist		10.40 (12.69)	6.44 (8.40)	6.43 (8.39)	**6.37** (**8.38**)
BMI		2.98 (3.86)	2.65 (3.39)	2.68 (3.46)	**2.50** (**3.30**)
SBP		15.62 (19.56)	11.11 (13.96)	11.21 (14.05)	**10.46** (**13.33**)
DBP		19.47 (22.05)	8.19 (10.27)	8.22 (10.29)	**7.74** (**9.88**)
Glucose		14.20 (20.27)	11.82 (19.01)	12.02 (19.13)	**11.33** (**18.32**)
HbA1c		0.91 (1.15)	0.43 (0.73)	0.41 (0.73)	**0.39** (**0.72**)
Creatinine		0.40 (0.44)	0.13 (0.18)	0.14 (0.18)	**0.11** (**0.16**)
BUN		2.91 (3.67)	2.73 (3.51)	2.59 (3.40)	**2.52** (**3.35**)
Total cholesterol		37.67 (47.76)	31.03 (39.35)	30.85 (39.35)	**30.46** (**38.91**)
Triglycerides		59.28 (77.98)	58.87 (77.55)	57.96 (77.10)	**49.72** (**75.88**)
Uric Acid		1.83 (2.21)	1.04 (1.33)	1.09 (1.37)	**0.93** (**1.19**)
# Params	–	3260M	133.2M	271.4M	**30.51M**
GFLOPS		426	18.8	65.8	**4.49**

Table 3: Performance comparison of w/ and w/o the proposed strategies. The **best** and second best results are highlighted in **bold** and underline, respectively.

	Metrics	SePL w/o MTL, Self-propagation	SePL w/o Self-propagation	SePL
Gender	Acc (AUC)	57.21% (0.50)	87.12% (**0.86**)	**87.30%(0.86)**
Age	MAE (RMSE)	5.37 (7.11)	3.43 (4.57)	**3.34** (**4.40**)
Height		7.28 (8.96)	5.62 (**7.10**)	**5.60** (7.12)
Weight		11.34 (13.86)	9.04 (11.87)	**8.99** (**11.80**)
Waist		6.57 (8.40)	6.41 (**8.35**)	**6.37** (8.38)
BMI		2.71 (3.47)	2.53 (**3.30**)	**2.50** (**3.30**)
SBP		11.87 (14.71)	10.60 (13.49)	**10.46** (**13.33**)
DBP		8.77 (10.94)	7.78 (9.95)	**7.74** (**9.88**)
Glucose		12.06 (20.57)	11.45 (19.20)	**11.33** (**18.32**)
HbA1c		0.42 (0.77)	0.40 (**0.72**)	**0.39** (**0.72**)
Creatinine		0.14 (0.19)	**0.11** (**0.16**)	**0.11** (**0.16**)
BUN		2.60 (3.53)	2.57 (3.48)	**2.52** (**3.35**)
Total cholesterol		30.86 (39.32)	31.32 (39.93)	**30.46** (**38.91**)
Triglycerides		52.79 (78.61)	50.33 (76.15)	**49.72** (**75.88**)
Uric Acid		1.13 (1.39)	0.94 (1.21)	**0.93** (**1.19**)
# Params	–	417.3M	**27.83M**	30.51M
GFLOPS		67.3	**4.49**	**4.49**

We further evaluate the proposed SePL to demonstrate the effect of MTL and self-propagation, as detailed in Table 3. The adoption of MTL improves the overall performance significantly with MAE 17.36% and RMSE 16.40% in average. In particular, gender and age represent 52.28% and 56.56% improvement in MAE. The large performance gains denote that shared feature extractor captures useful common features by leveraging cross-task correlations. However, MAE and RMSE of total cholesterol worsen 1.49% and 1.55%, indicating that total cholesterol is sensitive to the noise inherent in the individual tasks and

requires additional information for prediction. Self-propagation with DMoE fusion further improves MAE 1.21% and RMSE 1.27% in average across all CMR factors. Especially, contributed 9 factors show better performance improvement with MAE 1.39% and RMSE 1.69% in average, whereas 6 anthropometric factors represent average improvement of MAE 0.93% and RMSE 0.63%.

Acknowledgments. This work was partly supported by the Korea government (MSIT), IITP, Korea, under the ICT Creative Consilience program (IITP-2025-RS-2020-II201821, 30%), Development of Brain Disease (Stroke) Prediction Model based on Fundus Image Analysis (RS-2024-00459512, 30%), AI Innovation Hub (RS-2021-II212068, 20%), and AI Graduate School Program (Sungkyunkwan University, RS-2019-II190421, 20%).

Disclosure of Interests. The authors have no competing interests to declare that are relevant to the content of this article.

References

1. Aristizabal, J.C., Barona, J., Hoyos, M., Ruiz, M., Marín, C.: Association between anthropometric indices and cardiometabolic risk factors in pre-school children. BMC pediatrics **15**, 1–8 (2015)
2. Can, A.S., Bersot, T.P., Gönen, M.: Anthropometric indices and their relationship with cardiometabolic risk factors in a sample of turkish adults. Public Health Nutrition **12**(4), 538–546 (2009)
3. Danaei, G., Lu, Y., Singh, G.M., Carnahan, E., Stevens, G.A., Cowan, M.J., Farzadfar, F., Lin, J.K., Finucane, M.M., Rao, M., et al.: Cardiovascular disease, chronic kidney disease, and diabetes mortality burden of cardiometabolic risk factors from 1980 to 2010: a comparative risk assessment. The Lancet Diabetes and Endocrinology **2**(8), 634 (2014)
4. Ezinne, N.E., Roodal, D., Ekemiri, K.K., Persad, T., Mashige, K.P.: Ocular parameters and anthropometry in indo-trinidadians. Medicine **102**(52), e36763 (2023)
5. Gerrits, N., Elen, B., Craenendonck, T.V., Triantafyllidou, D., Petropoulos, I.N., Malik, R.A., De Boever, P.: Age and sex affect deep learning prediction of cardiometabolic risk factors from retinal images. Scientific reports **10**(1), 9432 (2020)
6. Khan, N.C., Perera, C., Dow, E.R., Chen, K.M., Mahajan, V.B., Mruthyunjaya, P., Do, D.V., Leng, T., Myung, D.: Predicting systemic health features from retinal fundus images using transfer-learning-based artificial intelligence models. Diagnostics **12**(7), 1714 (2022)
7. Kidy, F.F., Dhalwani, N., Harrington, D.M., Gray, L.J., Bodicoat, D.H., Webb, D., Davies, M.J., Khunti, K.: Associations between anthropometric measurements and cardiometabolic risk factors in white european and south asian adults in the united kingdom. In: Mayo Clinic Proceedings. vol. 92, pp. 925–933. Elsevier (2017)
8. Kim, H.T., Kim, J.M., Kim, J.H., Lee, J.H., Lee, M.Y., Lee, J.Y., Won, Y.S., Park, K.H., Kwon, H.S., Society, K.O.: Relationships between anthropometric measurements and intraocular pressure: the korea national health and nutrition examination survey. American Journal of Ophthalmology **173**, 23–33 (2017)
9. Kingma, D.P., Ba, J.: Adam: A method for stochastic optimization. arXiv preprint arXiv:1412.6980 (2014)

10. Liu, J., Tse, L.A., Liu, Z., Rangarajan, S., Hu, B., Yin, L., Leong, D.P., Li, W.: Predictive values of anthropometric measurements for cardiometabolic risk factors and cardiovascular diseases among 44 048 chinese. Journal of the American Heart Association **8**(16), e010870 (2019)
11. Liu, Z., Mao, H., Wu, C.Y., Feichtenhofer, C., Darrell, T., Xie, S.: A convnet for the 2020s. In: Proceedings of the IEEE/CVF conference on computer vision and pattern recognition. pp. 11976–11986 (2022)
12. Pölsterl, S., Gutiérrez-Becker, B., Sarasua, I.: Abhijit guha roy, and christian wachinger artificial intelligence in medical imaging (ai-med), department of child and adolescent psychiatry, ludwig maximilian universität, munich, germany. Adolescent Brain Cognitive Development Neurocognitive Prediction: First Challenge, ABCD-NP 2019, Held in Conjunction with MICCAI 2019, Shenzhen, China, October 13, 2019, Proceedings **11791**, 99 (2019)
13. Poplin, R., Varadarajan, A.V., Blumer, K., Liu, Y., McConnell, M.V., Corrado, G.S., Peng, L., Webster, D.R.: Prediction of cardiovascular risk factors from retinal fundus photographs via deep learning. Nature biomedical engineering **2**(3), 158–164 (2018)
14. Speechly, C., Bignell, N., Turner, M.: Sphygmomanometer calibration: why, how and how often? Australian family physician **36**(10) (2007)
15. Stevens, S.L., Wood, S., Koshiaris, C., Law, K., Glasziou, P., Stevens, R.J., McManus, R.J.: Blood pressure variability and cardiovascular disease: systematic review and meta-analysis. bmj **354** (2016)
16. Suter, Y., Knecht, U., Wiest, R., Reyes, M.: Overall survival prediction for glioblastoma on pre-treatment mri using robust radiomics and priors. In: Brainlesion: Glioma, Multiple Sclerosis, Stroke and Traumatic Brain Injuries: 6th International Workshop, BrainLes 2020, Held in Conjunction with MICCAI 2020, Lima, Peru, October 4, 2020, Revised Selected Papers, Part I 6. pp. 307–317. Springer (2021)
17. Vanuzzo, D., Pilotto, L., Mirolo, R., Pirelli, S.: Cardiovascular risk and cardiometabolic risk: an epidemiological evaluation. Giornale Italiano di Cardiologia (2006) **9**(4 Suppl 1), 6S–17S (2008)
18. Zhou, Y., Yu, H., Shi, H.: Study group learning: Improving retinal vessel segmentation trained with noisy labels. In: Medical Image Computing and Computer Assisted Intervention–MICCAI 2021: 24th International Conference, Strasbourg, France, September 27–October 1, 2021, Proceedings, Part I 24. pp. 57–67. Springer (2021)
19. Zuiderveld, K.J., et al.: Contrast limited adaptive histogram equalization. Graphics gems **4**(1), 474–485 (1994)